Evaluation of Results from Acoustic Emissions-Based Cavitation Monitor, Grand Coulee Unit G-24

Cavitation Monitoring System Comparison Tests, Grand Coulee Project

Final Report

Paul J. Wolff
WolffWare Ltd.

R. Keith Jones
River Operations
Tennessee Valley Authority

Patrick March
Hydro Performance Processes, Inc.

October 2005

EXECUTIVE SUMMARY

In an effort to evaluate cavitation monitoring technologies and to reduce cavitation damage on the Grand Coulee turbine runners, the U. S. Bureau of Reclamation (Reclamation) and Hydro Resource Solutions LLC (HRS) have initiated a multi-year research project under Cooperative Research and Development Agreement BOR-D9000-CRD-1043-HRS. The Tennessee Valley Authority (TVA) is supporting Reclamation on the project under an Interagency Services Agreement (01AA810712, Modification No. 01). A major task of the project is to investigate commercially available cavitation monitoring systems and to correlate the outputs of these systems with metal loss. This report presents analyses based on results obtained with the HRS AEM2000 acoustic emissions-based cavitation monitor.

Data were from the HRS AEM2000 cavitation monitor from unit G-24 over two inspection intervals; the first interval included data acquired from 5/8/2002 through 4/30/2003 while the second inspection interval included data from 5/1/2003 through 9/24/2004. The unit was inspected at the beginning and end of each interval to evaluate the cavitation damage that occurred in each interval.

One of the objectives of this project was to calibrate an empirical model quantifying metal loss as a function of the output of the HRS AEM2000 cavitation monitor. However, a reasonable fit to the data was not achieved because of several factors that include; inconsistencies in the inspection and data acquisition intervals; significant periods of time when cavitation data were not acquired; noise in the cavitation data; and errors in the metal loss estimates. Although the metal loss data did not result in a reasonable fit to the empirical model, the data and analyses in this report provide preliminary operating guidelines for reducing cavitation damage. Cavitation profiles showing the fractional erosion for each power level are largely insensitive to the fit coefficients. These profiles demonstrate that the cavitation damage is occurring at unit power outputs smaller than 450 MW which account for less than 3% of the unit's energy production.

BACKGROUND

Mechanisms for Cavitation Erosion and Acoustic Emissions

The cavitation erosion process resembles surface fatigue wear in which the surface is subjected to repeated, localized loading that produces surface and subsurface crack formation. Theoretical and experimental evidence has shown that the collapse of a cavitation bubble can produce a high velocity microjet (Tomita and Shima, 1986; Dear and Field, 1988), resulting in the eventual erosion of neighboring surfaces.

Cavitation produces vibrations in the cavitating fluid over a wide frequency range (Knapp et al., 1970; Lush and Hutton, 1976; Ramamurthy and Bhaskaran, 1979; De and Hammitt, 1982; Li et al., 1986; Abbot and Walsh, 1990). Acoustic emissions are the high

frequency vibrations resulting from localized, microscopic failures of material bonds which typically occur during plastic deformation in metals (Spanner, 1974). Cavitation erosion of a material produces acoustic emissions in the material (Jones and March, 1989; Jones et al., 1989; Derakhshan et al., 1990; March and Jones, 1991).

Measurement of Cavitation Level Using Acoustic Emissions

The AEM2000 Monitoring System detects the high frequency vibrations that occur during cavitation using an acoustic emission transducer. This transducer is typically glued and clamped to an exposed metal surface on the draft tube liner of a turbine runner, in close proximity to the throat ring. The installation for G-24 is shown in Figure 1. Signals from the transducer are filtered and amplified, and then provided as an input to a wideband RMS-to-DC converter chip. The converter chip computes the true RMS value of a complex waveform and gives an equivalent DC voltage output, thus producing an output directly related to the power of the signal. The DC voltage is normalized by the full scale voltage and recorded as a value between 0 and 100%.

Figure 1: AEM2000 Installation on G-24

Computations

Computing metal loss from a cavitation signal requires formulating and calibrating an equation that relates the cavitation signal to a metal erosion rate.

A series of laboratory tests performed at the Tennessee Valley Authority's Engineering Laboratory (Jones and March, 1989; Derakhshan et al., 1990; March and Jones, 1991) provide the basis for the cavitation equation used in this study. These tests utilized an apparatus that creates a cavitating jet which impinges on the test specimen. The cavitation level was measured by a high frequency accelerometer attached to the test specimen. Acoustic emissions data was acquired at a sampling rate of 10 MHz. The signal from the accelerometer was provided to a wideband RMS-to-DC converter chip, which computes the true RMS value of the signal and produces an output voltage that is linearly proportional to the RMS value. Each test run involved operating the cavitating jet apparatus at a fixed pressure and flow rate and exposing the metal specimen to the cavitating jet for a specified length of time. The metal specimen was weighed before and after exposure to the cavitating jet to determine metal loss. The log-linear plot shown in Figure 2 presents data relating metal loss to signal level from the acoustic emissions-based cavitation monitor (Jones and March, 1989; Derakhshan et al., 1990).

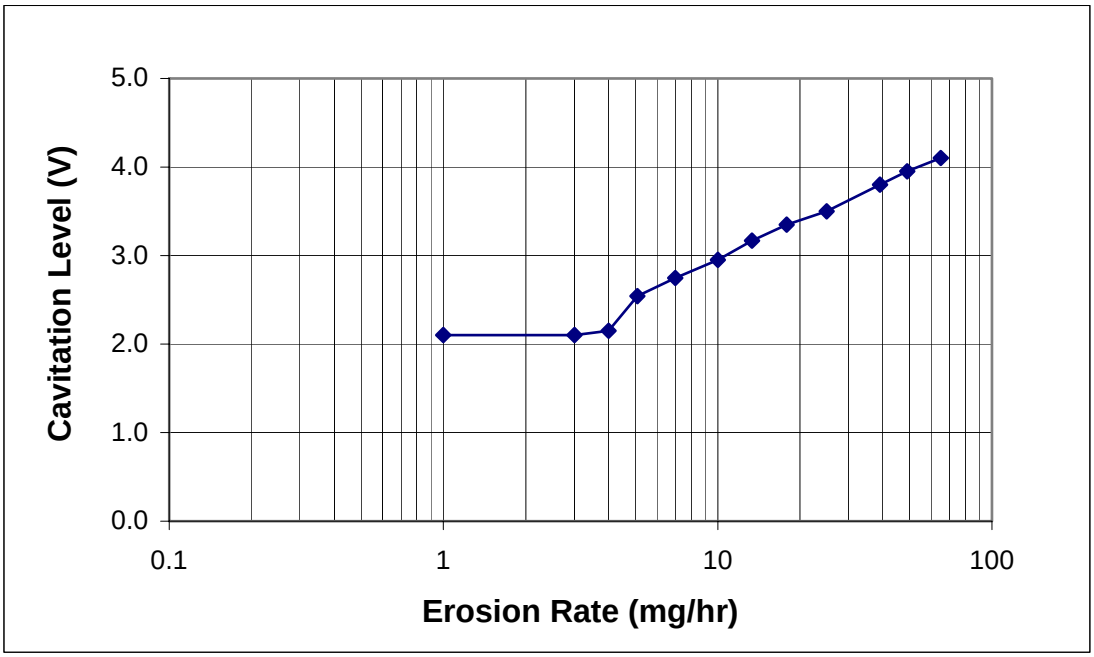

Figure 2: Laboratory Cavitation Measurements

Two lines can fit the data presented in Figure 2; the first line extends from an erosion rate of 1 to 4 mg/hr at a constant cavitation level of 2.1 V while the second line extends from 4 to 65 mg/hr with a constant slope on a log-linear plot. Based on this figure, it is clear that an exponential relationship will adequately fit most of the data. The following relationship was chosen to relate erosion rate to the measured cavitation level:

$$y = a(e^{b(x-x_0)} - 1) \qquad (1)$$

where

y = erosion rate
x = cavitation level
a, b, x_0 = calibration coefficients.

Equation 1 contains an offset of x_0 for the cavitation level. This is based on observations of cavitation data that displayed a minimum cavitation output over the entire range of operating conditions. Because this minimum cavitation signal appears to be produced largely by background noise, it is subtracted from the measured cavitation signal. The relation shown in equation 1 fits most of the data presented in Figure 2 and produces an erosion rate of 0 when the cavitation signal is equal to the minimum level of x_0.

Although Equation 1 produces a reasonable fit to the laboratory cavitation data, more transducers may be required for accurately predicting prototype cavitation erosion rates. There are many cavitation mechanisms that may occur simultaneously, at differing locations, in a prototype (Bajic, 2003). Each mechanism produces a different erosion rate and measuring the different mechanisms would require several transducers mounted at different axial and circumferential locations on the turbine housing.

Calibration of the Model

Equation 1 contains 3 fit coefficients, x_0, a, and b. As previously stated, the first coefficient is obtained directly from a plot displaying the cavitation levels versus power and head. To obtain the fit coefficients a and b, data must be continuously acquired over inspection intervals in which the amount of metal loss due to cavitation erosion is quantified. Because there are two fit coefficients, data from a minimum of two inspection intervals is necessary. However, due to measurement uncertainties that include noise in the cavitation signal and the difficulty in accurately determining metal loss from one inspection interval to the next, data from multiple inspections would improve the accuracy of the fit coefficients.

Computing the calibration coefficients first requires that the metal loss be related to the erosion rate:

$$Y_c = \int_{t_0}^{t_1} a(e^{b(x-x_0)} - 1)dt \qquad (2)$$

where

Y_c = computed metal loss
t_0, t_1 = beginning and ending times of inspection interval.

The next step involves computing an error term to fit the data to the model with a least squares approach:

$$E = \sum_{i=1}^{i=n} (Y_{m_i} - Y_{c_i})^2 \quad (3)$$

where

Ym = measured metal loss
i = maintenance interval
n = number of inspection intervals.

Because the functional form of x is unknown, Yc and therefore E do not have closed form solutions and must be computed with numerical techniques. The numerical solution involves computing a cavitation history for each maintenance interval. The cavitation history is computed by summing the time the unit operated in discrete cavitation intervals ranging from the minimum to maximum cavitation level. For this study, the cavitation interval ranged from 0 to 100% with an interval of 0.5%. Given the cavitation history and the calibration coefficients *a*, *b*, and x_0, the metal loss can be computed with numerical integration based on the rectangle rule:

$$Y_c = a \sum_{j=1}^{j=m} t_j * (e^{b(x_j - x_0)} - 1) \quad (4)$$

where

j = cavitation bin
m = number of bins in cavitation matrix
t_j = the time the unit operated in the in the jth interval
x_j = the nominal cavitation level for the jth interval, taken to be the average of the data in the interval

If *a* and *b* are unknown, and two or more inspection intervals exist, the cavitation matrices in conjunction with Equations 3 and 4 can be used to compute *a* and *b*.

Computing Cavitation Erosion Profiles

Because inspections are performed infrequently, obtaining sufficient data to compute the calibration coefficients may require several years. However, the fractional amount of erosion that occurs at each operating point can be readily computed with data from a single maintenance interval. The fractional erosion is computed using the following equation:

$$y_k = \frac{t_k * (e^{b(x_k - x_0)} - 1)}{\sum_{j=1}^{j=m} t_j * (e^{b(x_j - x_0)} - 1)} \quad (5)$$

where

y_k = fraction of cavitation erosion occurring in kth cavitation bin
n_k = the number of data points in kth cavitation bin.

RESULTS

The results presented below are based on the data for two inspection intervals. The first interval is based on data acquired during the time period from 5/8/2002 through 4/30/2003 and the second is based on data acquired from 5/1/2003 through 9/24/2004. The data for the time period from 5/8/2002 through 5/16/2002 were acquired on a 15 minute sampling frequency while all other data were acquired on a 5 second sampling frequency.

The first major component of this analysis involved evaluating the dependence of the cavitation signal on the power and gross head levels. For the analysis of the data from the first inspection interval, data were averaged into head intervals ranging from 270 to 340 ft in 10 ft increments and in power intervals ranging from 0 to 850 MW in 10 MW increments. Figure 3 presents cavitation level versus unit power for the four head intervals that contained valid cavitation signals: 300 to 310, 310 to 320, 320 to 330, and 330 to 340. Figure 3 also contains error bars for each point, corresponding to the precision error of each averaged value. The precision errors are relatively low, indicating that for a given head and power interval the scatter in the data is reasonably small.

Figure 3 indicates that the cavitation level is a function of both head and power. The cavitation peaks at power levels of approximately 200 MW for each head level. The cavitation increases at this peak as the head increases. For power outputs greater than 400 MW the cavitation signal levels off to approximately 10%, which is close to the value of background noise. Figure 3 also shows that for power outputs greater than 550 MW the cavitation increases slightly as the head decreases. The lowest head of 305 ft produces the largest cavitation signal.

Cavitation levels from the second inspection interval are presented in Figure 4. These data demonstrate more scatter than data from the first inspection interval. This is partly shown by the larger error bars. In an effort to reduce the scatter in the data, the head interval was reduced from 10 to 5 ft. Figure 4 only displays data from every other head interval to enhance readability of the graph.

Figure 4 shows that the trends of cavitation level versus power are similar to the trends occurring in the first interval. There is a peak at approximately 200 MW and low cavitation levels are observed at power outputs greater than 500 MW. The dependence of cavitation on head is not as distinct in Figure 4. For power outputs less than 400 MW there is no clear dependence of cavitation level on head. For power outputs greater than 500 MW cavitation level is low and it increases slightly as the head decreases.

A possible problem with the cavitation data is that the level drops from the first to the second inspection interval. The cavitation signal for the first inspection interval approached magnitudes of 70% for power levels near 200 MW at a head of 335 ft. Similar power and head levels for the second inspection intervals produced cavitation levels of only 50%. It is not clear what produced the drop in the cavitation signal. The

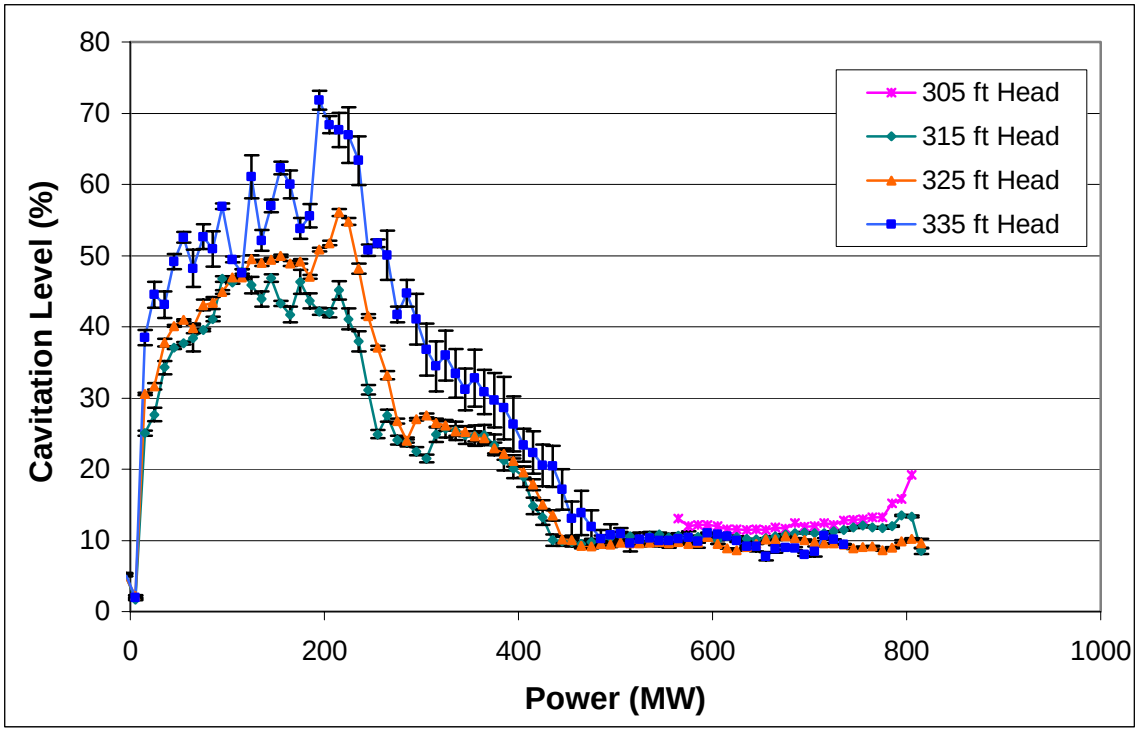

Figure 3: Field Cavitation Measurements versus Power and Head, First Inspection Interval

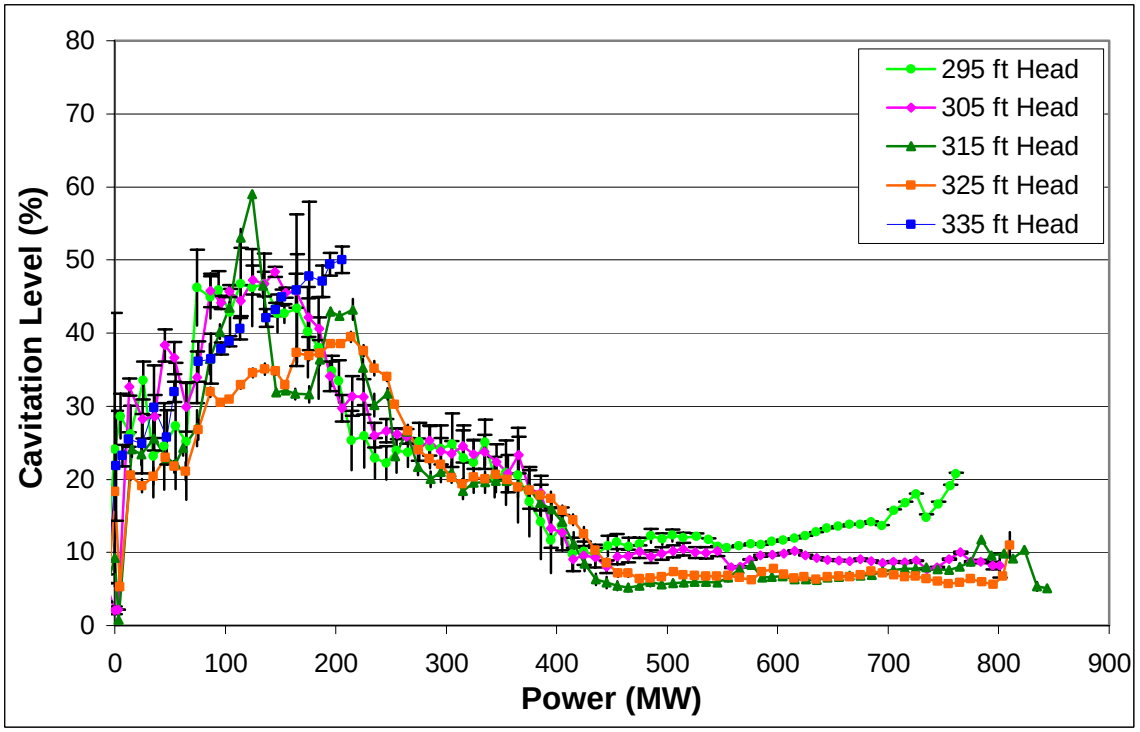

Figure 4: Field Cavitation Measurements versus Power and Head, Second Inspection Interval

unit was not modified between the first and second inspection intervals. In addition, conversations with plant personnel indicated that there were no recorded changes made to the cavitation instrumentation.

Previous flow cavitation studies conducted by Voith-Siemens Hydro on a physical model of the Grand Coulee runner help to confirm the validity of the cavitation curves presented in Figures 3 and 4. These cavitation studies were conducted at a model head level that corresponds to a prototype gross head of 285 ft. The cavitation and efficiency curves for the prototype at this head are presented as a function of power in Figure 5. The cavitation curve shown is based on a visual extrapolation of the cavitation data from the first inspection interval. The efficiency curve was obtained from unit characteristics based on the model study and scaled to the prototype. Also shown on this figure are labels referencing photographs from the model obtained at homologous operating points. The photographs are taken at the exit of the runner looking up into the runner.

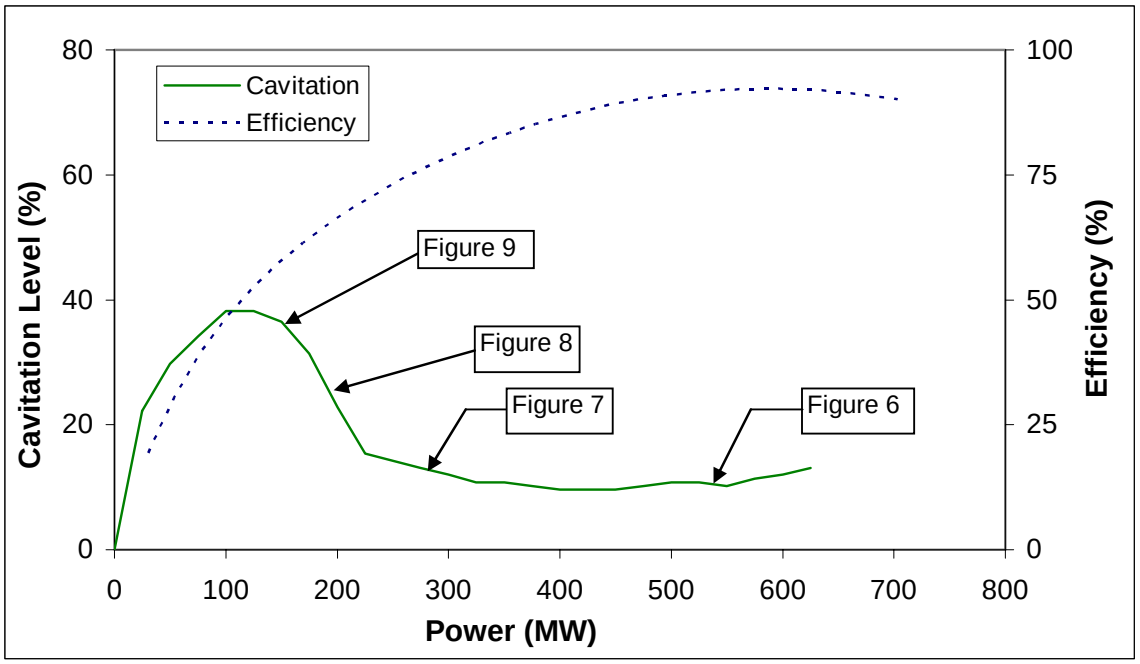

Figure 5: Cavitation and Efficiency Curve, Head = 285 ft

The five photographs in Figures 6 - 9 visually confirm that the acoustic emissions-based cavitation measurements acquired from the prototype correspond to cavitating flow conditions in the model. Figure 6 presents a reference photograph displaying operation near the best efficiency point with almost no visible cavitation, indicating that the runner is operating in a cavitation-free region. Figures 7 - 9 present photographs corresponding to operating points of 250, 175, and 150 MW, respectively. These operating points correspond to the lower portion of the measured cavitation curve, which contained relatively high signal levels from the cavitation monitor. Cavitating flow can be observed

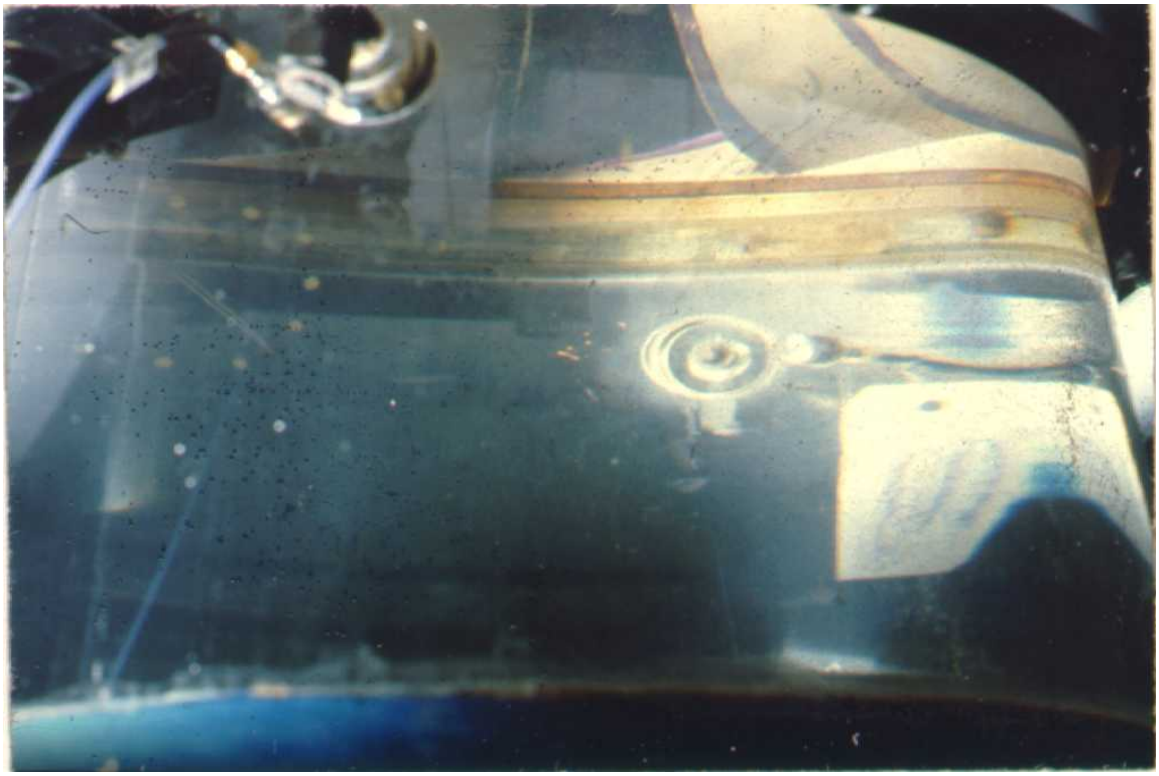

Figure 6: Model Runner, Prototype Power 575 MW, No Cavitation

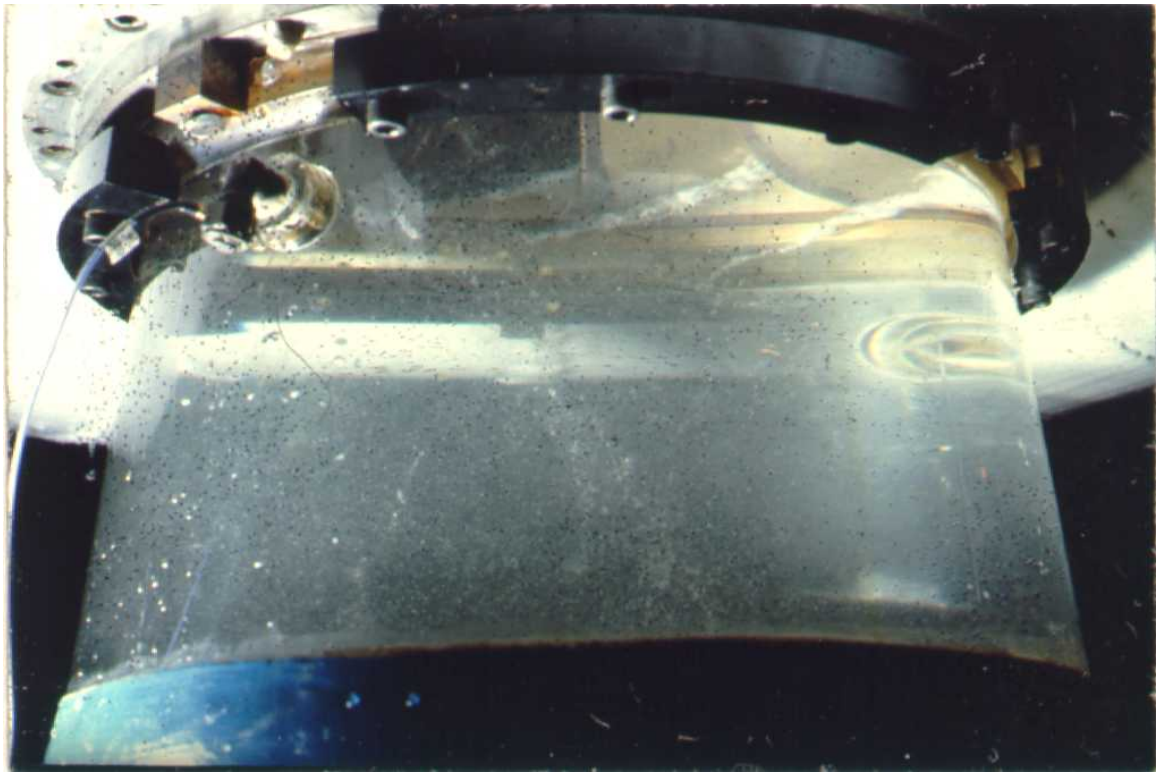

Figure 7: Model Runner, Prototype Power 250 MW, With Cavitation

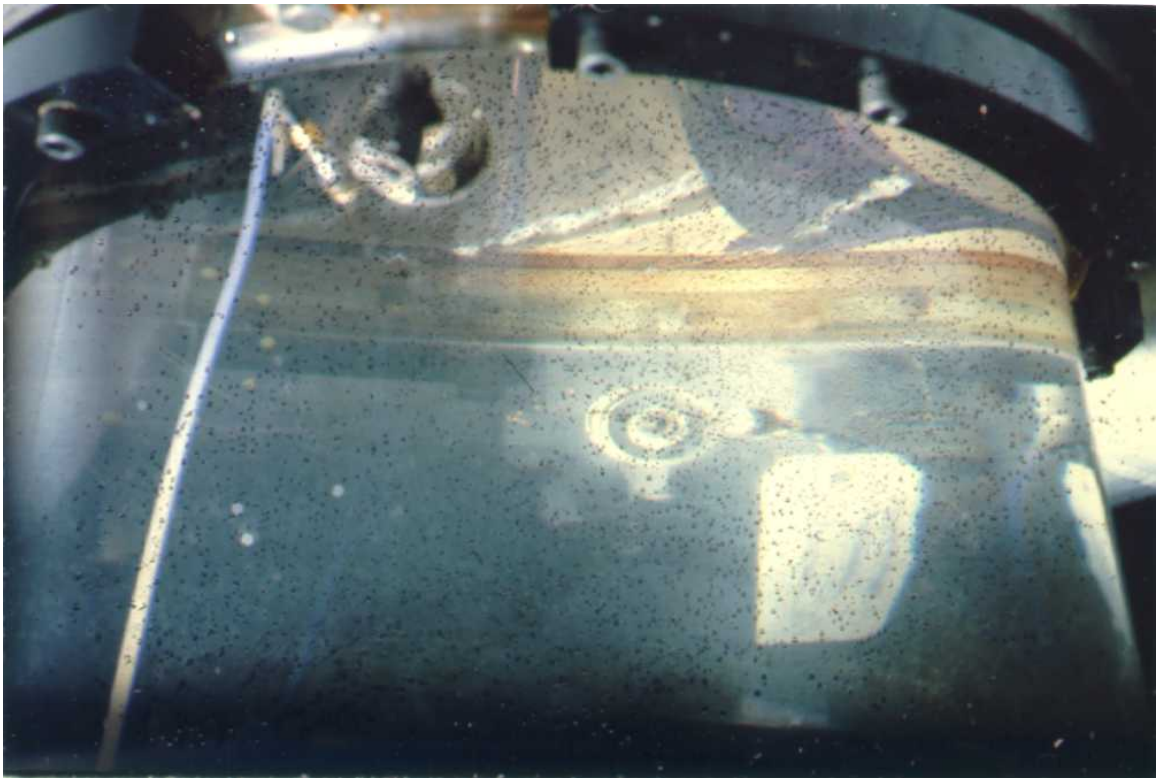

Figure 8: Model Runner, Prototype Power 175 MW, With Cavitation

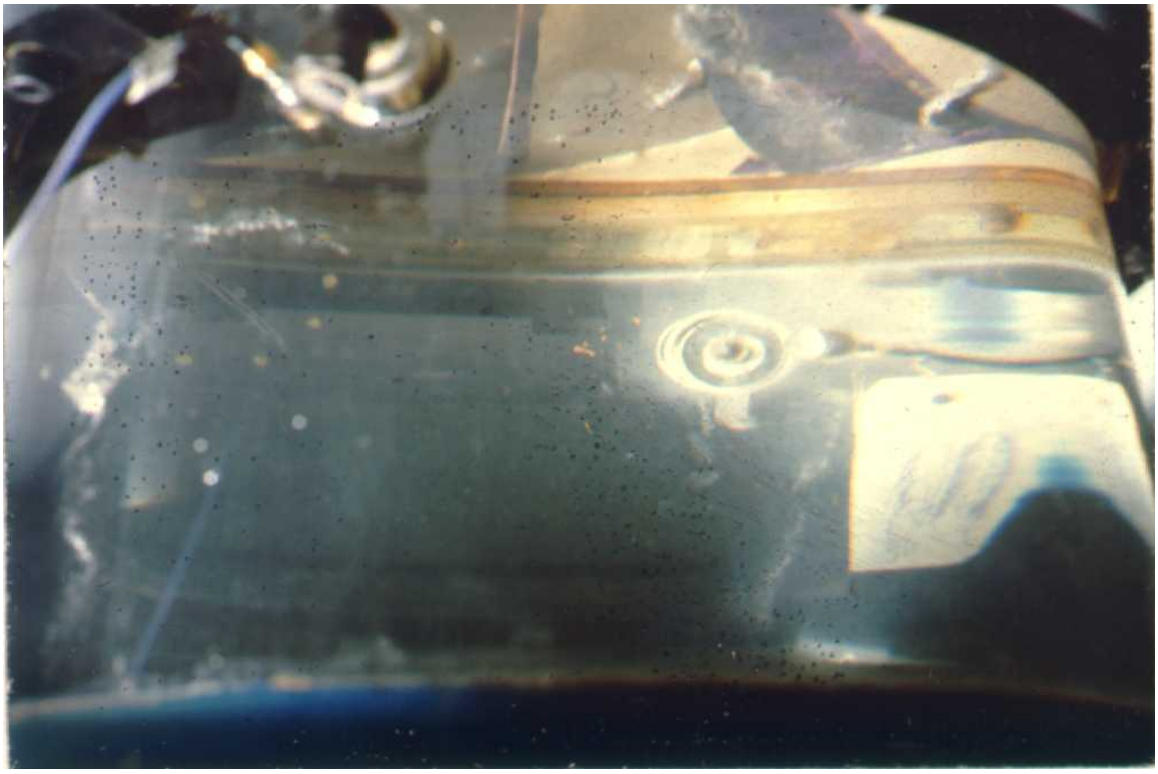

Figure 9: Model Runner, Prototype Power 150 MW, With Cavitation

in each of these figures, as shown by the vortex core and stream of cavitation bubbles attached to the runner's edge in the upper right-hand portion of each photograph.

Cavitation histories are presented in Figure 10 on a log-linear plot. The cavitation history is a summation of the operating times for each discrete cavitation interval between 0 and 100% with a resolution of 0.5%. In general, the cavitation history in the second inspection interval is smaller than the first interval. One of the factors for this could be the unexplained drop in cavitation level that occurred in the second cavitation interval. The cavitation history is not shown for levels less than 10% because this signal level was attributed to background noise.

Figure 11 displays the results of a sensitivity analysis. Cavitation data from both inspection intervals were averaged into 10 MW power intervals ranging between 0 and 850 MW. The fractional erosion for each power interval was then computed based on Equation 5 for three different values of *b*; .1, .01, and .001. Figure 11 presents the cavitation profiles for each value of *b*, and the energy profile. This figure shows that the cavitation erosion is occurring at power levels less than 450 MW while most of the energy generation, 98%, is produced at power levels greater than 450 MW.

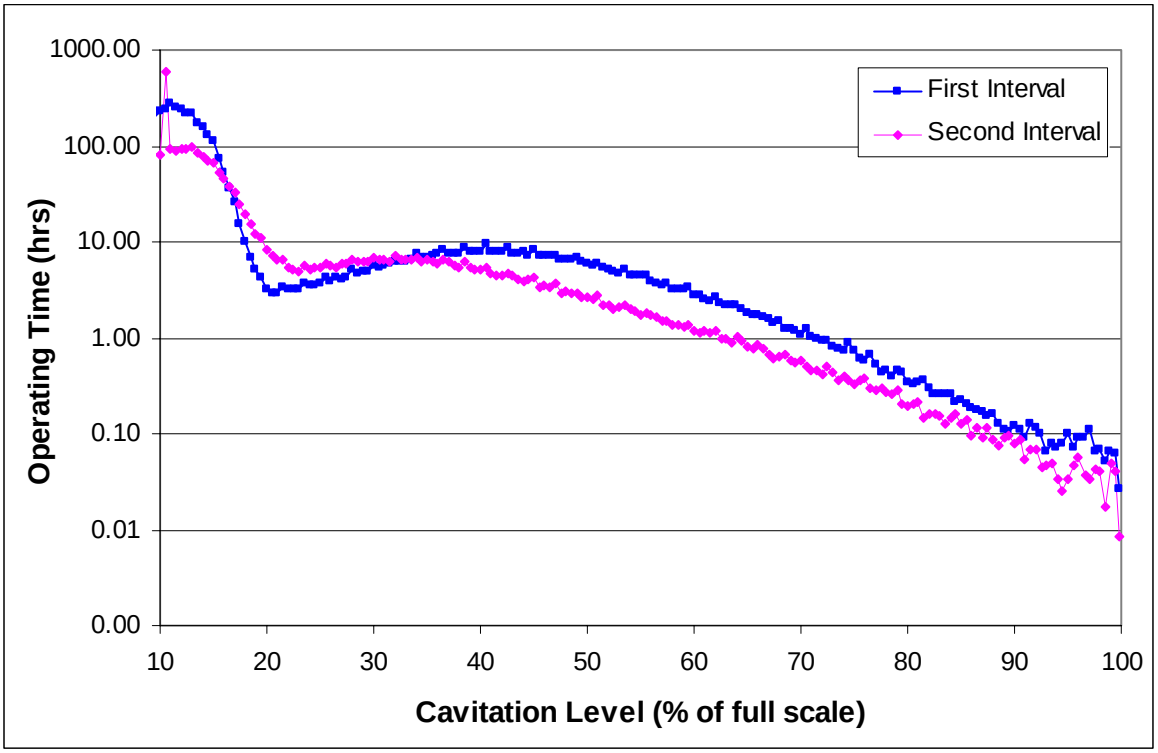

Figure 10: Cavitation Histories for Both Inspection Intervals

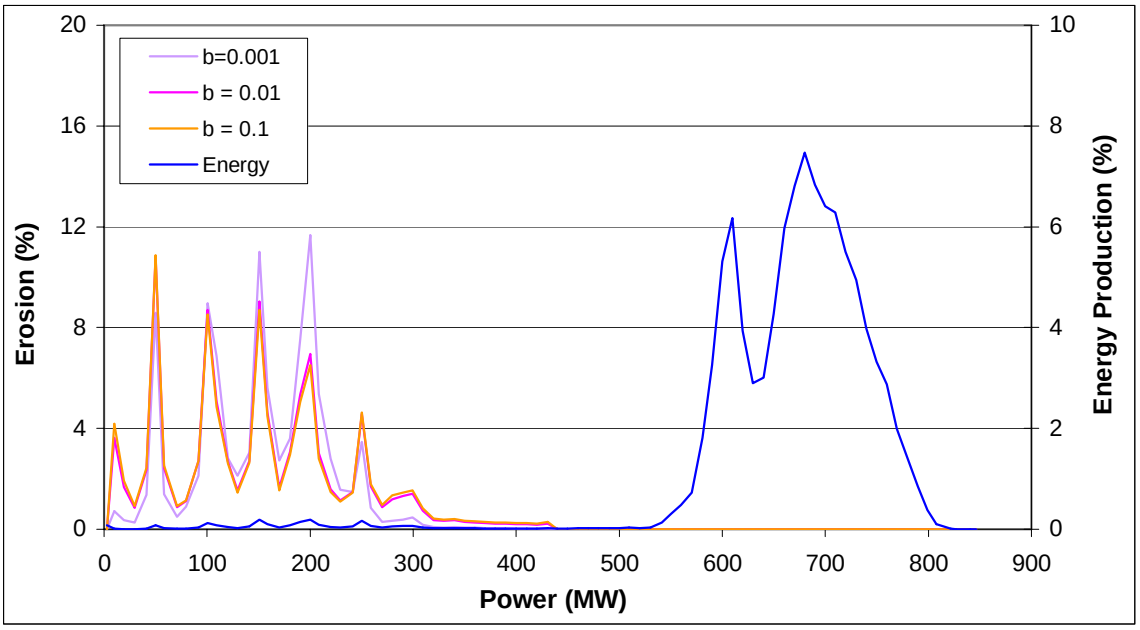

Figure 11: Cavitation Erosion versus Power

CONCLUSIONS AND RECOMMENDATIONS

Cavitation data were analyzed from data acquired during two inspection intervals. The first interval was based on data acquired during the time period from 5/8/2002 through 4/30/2003 and the second was based on data acquired from 5/1/2003 through 9/24/2004. Analyses of the cavitation data versus head and power clearly show that cavitation level depends on unit power. Data from the first inspection interval demonstrated that cavitation level also depended on head, but the correlation is not as apparent for the second inspection interval.

Cavitation and energy profiles computed from these data indicate that the cavitation damage is occurring at power levels less than 450 MW. Only 2% of the energy is generated at these same power levels. The cavitation data and analyses indicate that if energy generation at power levels less than 450 MW could be eliminated or reduced, cavitation damage would also be reduced.

More data and experience is necessary to validate and calibrate the cavitation monitoring system. The data and analyses in this report indicate that cavitation damage could be significantly reduced if unit G-24 were not operated at power levels less than 450 MW. If G-24 has sufficient operating flexibility, a test could be designed to validate this conclusion. The test would consist of the following steps; 1) perform a pre test evaluation of cavitation damage; 2) operate the unit for a significant period of time in which operation at power levels less than 450 MW is avoided; and 3) perform a post test evaluation of cavitation damage. Once the cavitation system is validated, it may be possible to calibrate the system to quantify metal loss versus cavitation level. This would

require cavitation erosion measurements for multiple inspection intervals in conjunction with continuous cavitation data. With a reasonable calibration, the cost of cavitation damage at any power level could be quantified.

ACKNOWLEDGEMENTS

Assistance and support was provided by the management and staff of Reclamation's Grand Coulee Project, particularly Michael Strombach and Randy Spotts. Photographs and data from the manufacturer's physical model study of the Grand Coulee turbines were provided by Voith-Siemens Hydro Power Generation Inc., whose assistance is gratefully acknowledged.

REFERENCES

Abbot, P. A., and J. Walsh, 1990, "Acoustic Cavitation Tests and Analyses of Pump-Turbine Unit 9 at the Lewiston Pump Generation Plant," Technical Memorandum No. 002, Falmouth, MA: Ferranti O.R.E., Inc.

Bajic, Branko, "Methods for Vibro-Acoustic Diagnostics of Turbine Cavitation," Journal Of Hydraulic Research, Vol. 41, 2003, No. 1.

De, M. K., and F. G. Hammitt, 1982, "New Method for Monitoring and Correlating Cavitation Noise to Erosion Capability," Transactions of the ASME Journal of Fluids Engineering, Volume 104, pp. 434-442.

Derakhshan, O., J. R. Houghton, R. K. Jones, and P. A. March, 1990, "Cavitation Monitoring of Hydroturbines with True-RMS Acoustic Emission Measurement," ASTM Special Publication 1077, Philadelphia: American Society for Testing and Materials.

Dear, J. P., and J. E. Field, 1988, "A Study of the Collapse of Arrays of Cavities," Journal of Fluid Mechanics, Vol. 190, pp. 409-425.

Jones, R. K., and P. A. March, 1989, "Application of Acoustic Emissions for Real-Time Monitoring of Cavitation," TVA Report No. WR28-4-900-234, Norris, Tennessee: Tennessee Valley Authority.

Jones, R. K., P. A. March, and J. M. Epps, "Monitoring Hydroturbines for Efficiency and Cavitation," Hydro Review, June 1989, pp. 72-79.

Knapp, R. T., J. W. Dailey, and F. G. Hammitt, 1970, Cavitation, New York: McGraw-Hill Book Company.

Li, S., Y. Zhang, and F. G. Hammitt, 1986, “Characteristics of cavitation bubble collapse pulses, associated pressure fluctuations, and flow noise,” Journal of Hydraulic Research, Vol. 24, pp. 109-122.

Lush, P. A., and S. P. Hutton, 1976, “The Relation between Cavitation Intensity and Noise in a Venturi-Type Section,” Proceedings of the International Conference on Pump and Turbine Design, Glasgow, Scotland.

March, P. A., and R. K. Jones, “Laboratory and Field Experience with Cavitation Monitoring of Hydroturbines,” Proceedings of Waterpower 91, July 1991.

Ramamurthy, A. S., and P. Bhaskaran, 1979, “Velocity Exponent for Erosion and Noise Due to Cavitation,” Transactions of the ASME Journal of Fluids Engineering, Volume 101, pp. 69-75.

Spanner, J.C., 1974, Acoustic Emission Techniques and Applications, Evanston, Illinois: Intex.

Tomita, Y., and A. Shima, 1986, “Mechanisms of impulsive pressure generation and damage pit formation by bubble collapse,” Journal of Fluid Mechanics, Volume 169, pp. 535-564.